Inorganic Chemistry

ARTICLE

pubs.acs.org/IC

Isomerism of [^{64}Cu-NOTA-Bn]-Labeled Radiotracers: Separation of Two Complex Isomers and Determination of Their Interconversion Energy Barrier Using Ion Pair Chromatography

Joern Schlesinger,[*,†,⊥] Johan Rajander,[‡,⊥] Janne A. Ihalainen,[§] Dinesh Ramesh,[†,⊥] Patrik Eklund,[∥] Veronica Fagerholm,[†,⊥] Pirjo Nuutila,[†,⊥] and Olof Solin[†,⊥]

[†]Turku PET Centre, University of Turku, Kiinamyllynkatu 4-8, 20520 Turku, Finland

[‡]Accelerator Laboratory, Åbo Akademi University, Porthansgatan 3, 20500 Turku, Finland

[§]Nanoscience Center, Department of Biological and Environmental Science, University of Jyväskylä, P.O. Box 35, 40014 Jyväskylä, Finland

[∥]Laboratory of Organic Chemistry, Åbo Akademi University, Piispankatu 8, 20500 Turku, Finland

[⊥]Centre of Excellence in Molecular Imaging in Cardiovascular and Metabolic Research, University of Turku, 20520 Turku, Finland

Supporting Information

ABSTRACT: The model complex $[^{64}Cu((S)\text{-}p\text{-}NH_2\text{-}Bn\text{-}NOTA)]^-$ ($[^{64}Cu]\mathbf{1}$) was used to study the isomerism of [^{64}Cu-NOTA-Bn]-labeled radiotracers. Two complex isomers $[^{64}Cu]\mathbf{1a}$ and $[^{64}Cu]\mathbf{1b}$, which were formed at a ratio of 1:9 during the complexation of $[^{64}Cu]Cu^{2+}$ with (S)-p-NH_2-Bn-NOTA, were separated using ion pair chromatography. To study the interconversion, the nonradioactive complex isomers Cu**1a** and Cu**1b** were separated and thermally treated at 90 °C in both ammonium acetate solution and deionized water. A faster interconversion rate was observed for both isomers with lower concentrations of ammonium ions. At the end of reaction, the thermodynamic Cu**1a** to Cu**1b** equilibrium ratio was 6:94. The particular energy barriers of the interconversion for Cu**1a** and Cu**1b** were 130 kJ mol^{-1} and 140 kJ mol^{-1}. Spectrophotometric measurements with Cu**1a** and Cu**1b** revealed two isomers adopting different geometrical configurations.

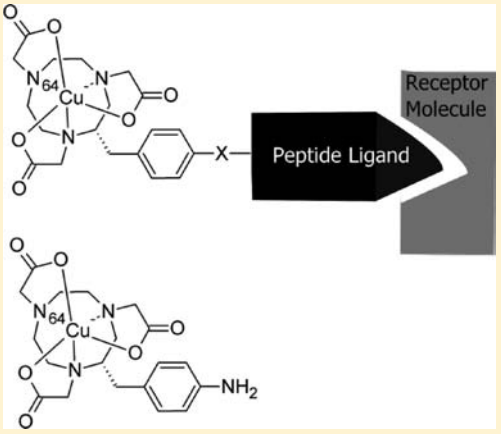

INTRODUCTION

In the recent past, radiometal-labeled agents acting as specific receptor ligands have gained importance in molecular imaging and diagnosis of various diseases.[1,2] On account of this, ^{64}Cu is a useful radionuclide for high resolution positron emission tomography (PET) imaging, because of its favorable properties and suitable decay characteristic ($t_{1/2}$ = 12.7 h, β^+_{max} 0.655 MeV, 17.4%). ^{64}Cu is routinely conjugated to targeting molecules using the bifunctional chelator approach.[3] In this context, the kinetic stability of the ^{64}Cu complex is a significant parameter for designing a ^{64}Cu-labeled agent. A suitable chelator for ^{64}Cu would be the macrocyclic compound 1,4,7-triazacyclononane-N,N',N''-triacetic acid (NOTA). It was shown recently that bifunctional chelators, based on NOTA, can be used to prepare kinetically inert ^{64}Cu-labeled agents.[4,5] Figure 1 shows examples of NOTA derivatives, which were previously used as bifunctional chelators.[4−7] The reactive functionality that serves as a linker to the targeting molecule can be introduced to the NOTA framework either at the ethylene bridge or via a chemical activation of a free carboxylate group of NOTA.

Isomerism of the ^{64}Cu-complex is another significant parameter for designing a radiometal-labeled agent. So far, little attention has been paid to the isomerism of radiometal complexes at the tracer level.[8] From that point of view, different isomeric chelates may have different physicochemical properties that affect their suitability for, or their behavior in, in vivo applications. The aim of this work was to study the chemical properties of the $[^{64}Cu((S)\text{-}p\text{-}NH_2\text{-}Bn\text{-}NOTA)]^-$ complex at the tracer level to understand its possible impact on the biological properties of [^{64}Cu-NOTA-Bn]-labeled radiotracers (Figure 2). For the first time, we report on the isomerism which was observed for the $[^{64}Cu((S)\text{-}p\text{-}NH_2\text{-}Bn\text{-}NOTA)]^-$ complex. Two different isomers, that were formed during the complexation of $^{64}Cu/Cu^{2+}$ with (S)-p-NH_2-Bn-NOTA, were analyzed

Received: August 31, 2010
Published: April 13, 2011

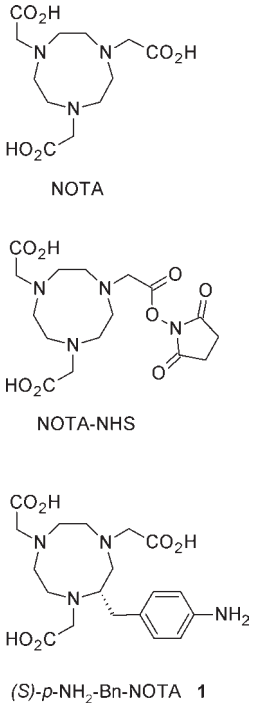

Figure 1. Bifunctional chelators based on the NOTA framework.

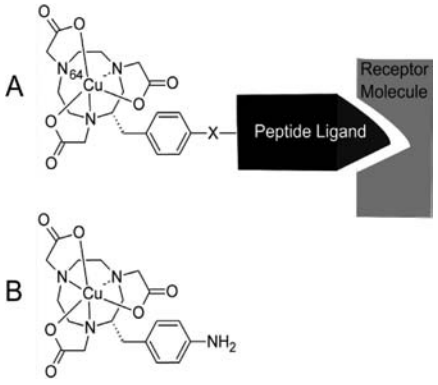

Figure 2. (A) Schematic illustration of a ^{64}Cu-labeled agent for in vivo receptor targeting by PET. (B) The nonradioactive complex $[Cu((S)\text{-}p\text{-}NH_2\text{-}Bn\text{-}NOTA)]^-$ (Cu**1**) was used to study the conformational isomerism of the chelate unit $[^{64}Cu]$**1**.

by ion pair chromatography, mass spectrometry, and UV−vis spectroscopy to obtain information about their structural differences. The free energy barriers and the activation parameters of the interconversion of the $[Cu((S)\text{-}p\text{-}NH_2\text{-}Bn\text{-}NOTA)]^-$ complex isomers were determined using ion pair chromatography.

EXPERIMENTAL SECTION

Chemicals and Materials. High effective specific activity (ESA) of ^{64}Cu was produced at Turku PET Centre, Finland, as previously described.[9] (*S*)-2-(4-Aminobenzyl)-1,4,7-triazacyclononane-*N*,*N*′,*N*″-triacetic acid (**1**) was obtained from Macrocyclics (U.S.A.). NH_4OAc (TraceSelect) was purchased from Sigma-Aldrich. Water was deionized (18.2 MΩ/cm^2) by passing it through the water filtration system Ultra Clear (SG, Germany).

All reactions and incubations were performed in 1.5 mL PP tubes (Eppendorf, Germany). Incubations were performed on a ThermoCell MB-102 (Biostep, Germany) and Thermomixer Comfort (Eppendorf, Germany). The temperature accuracy of both thermomixers was measured with a digital multimeter (FLUKE 179, Fluke, Finland) equipped with a thermocouple. Lyophilization was carried out using an ALPHA 2-4 LCS (Christ, Germany) freeze-dryer. Evaporation of liquid samples was performed with a vacuum concentrator (RVC 2-18, Christ, Germany), using the freeze-dryer ALPHA 2-4 LCS as a cooling trap. Measurements of pH values were done with the pH sensor Biotrode (Metrohm, Germany) or with the inLab MicroElectrode (Mettler Toledo, U.S.A.). Centrifugation was performed in the fixed-angle rotor centrifuge Sigma 1-14 (Sigma Laborzentrifugen, Germany) at room temperature. Radioactivity was scaled with a VDC-405 dose calibrator (Veenstra Instruments, Netherlands).

Chromatographic Purification and Analysis. HPLC purifications were performed using a HITACHI pump L-6220 (Japan) coupled with an L-2400 UV-detector (VWR, Finland). HPLC analyses were performed with a LaChrom Elite system using EZChrom Elite software (VWR, Finland). The system consisted of an L-2130 pump and L-2400 UV-detector. The HPLC columns were the following: (A) Synergy Hydro-RP column (Phenomenex, U.S.A.) 250 × 4.6 mm, 4 μm, coupled with a SecurityGuard AQ C18 cartridge (Phenomenex, U.S.A.) 3.0 × 4.0 mm, (B) μBondapak C18 (Waters, U.S.A.) 300 × 7.8 mm, 4 μm. HPLC mobile phases were (I) H_2O/CH_3CN (95:5 v/v), (II) 50 mM NH_4OAc buffer (pH 6.0) containing 5% CH_3CN, (III) 50 mM triethylammonium acetate (TEAA) buffer (pH 6.0) containing 5% CH_3CN. System A(I) and A(II): flow 0.75 mL/min, UV 240 nm, isocratic 0−25 min. System A(III): flow 0.75 mL/min, UV 240 nm, isocratic 0−45 min. System B(II): flow 2 mL/min, UV 300 nm, isocratic 0−20 min.

Thin layer chromatography (TLC) analyses were performed on silica gel plates (K60, Merck, Germany) with a mobile phase consisting of a mixture of 50 mM NH_4OAc and MeOH (1:1 v/v). The nonradioactive compounds were visualized under UV light at 254 nm (CAMAG, Germany). The radioactive compounds were visualized by exposing the dried TLC plates to a phosphor imaging plate and scanning this plate with the FLA-5100 image reader (FUJIFILM, Japan). Radiochemical yields were calculated from the activity area of the product peak related to the total activity area using Tina 2.09 software (Raytest, Germany).

Solid phase extraction (SPE) was performed on a Strata-X AW (30 mg) cartridge (Phenomenex, U.S.A.) with primary and secondary amine functionalities. The elution profiles of chelator **1** and the complex Cu**1** were initially monitored using an ÄKTAprime plus system (GE Healthcare, Germany) by applying a linear gradient method (Supporting Information, Table 1S). The mobile phases were: (A) DI water and (B) an aqueous 0.1% TFA solution. Compound **1** (0.25 μmol) and Cu**1** (0.1 μmol) were dissolved each in 250 μL of NH_4OAc buffer (0.5 M). UV profiles (254 nm) were evaluated with PrimeView software (GE Healthcare, Germany) (Supporting Information, Figures 6S and 7S).

Mass Spectrometry. Mass spectra were recorded on a 4000 Q TRAP ESI-MS system (Applied Biosystems, U.S.A.) and analyzed using the program Analyst 1.4 (Applied Biosystems, U.S.A.).

NMR Studies. One-dimensional (1D) and two-dimensional (2D) spectra were recorded on a Bruker AV 500 spectrometer (Bruker, U.S.A.) using standard pulse sequences. 3-(Trimethylsilyl)propionic acid-d_4 sodium salt was used as an internal standard.

Spectrophotometric Measurements. For spectrophotometric analyses, aqueous stock solutions of Cu**1a** and Cu**1b** were prepared by dissolving Cu**1a** (2.7 mg) and Cu**1b** (4.7 mg) in 285 and 500 μL of DI water, respectively. For sample preparation, the stock solutions were diluted with DI water in ratios stated below. The pH of the aqueous Cu**1a** and Cu**1b** solutions was determined in 1:10 diluted samples and was pH 5.0 in both samples.

UV−vis measurements were performed on a Lambda 850 spectrophotometer (Perkin-Elmer, U.S.A.). The experiments were carried out

at room temperature using a Hellma 114B-QS cuvette (Hellma GmbH, Germany) with an optical path length of 1 cm. Measurements in the region 500−900 nm were done with 1:10 diluted samples. Measurements in the region 190−700 nm were done with a 1:500 diluted sample of Cu**1a** and a 1:600 diluted sample of Cu**1b**. All absorption spectra were scaled to the concentration. This leads to the absorption coefficient unit $1/cm(mM)^{-1}$. The overlapping of all absorption spectra in the region 500−700 nm is shown in Supporting Information, Figure 10S.

Circular dichroism (CD) spectroscopy was performed on a J-715 spectropolarimeter (Jasco, Japan) interfaced with a personal computer. The CD spectra were acquired and processed using the J-700 program (Jasco, Japan) for Windows. The experiments were carried out at room temperature using quartz cells (Hellma GmbH, Germany) with Suprasil windows and an optical path length of 0.05 cm. Analyses were performed on 1:20 diluted samples in the wavelength range of 190−400 nm using two different parameter sets P1 and P2 (Supporting Information, Table 2S, Figure 11S). The signal-to-noise ratio was improved by accumulating 8 and 4 scans respectively. Additionally, the spectra, measured with the different parameter sets were averaged.

NH_4^+ Ion-Selective Measurements. The analytic system (Nico2000, U.K.) consisted of an NH_4^+ ion-selective electrode (ELIT 8051) and a LiCl reference electrode (ELIT 003). Both electrodes were plugged into a dual electrode head (ELIT 201) and connected to a pH meter (pH 213, HANNA instruments, U.S.A.). For preconditioning, the NH_4^+ ion-selective electrode was immersed in a 55 mM NH_4OAc solution (pH 6.7) at room temperature for 5−7 days. An NH_4OAc stock solution (55 mM, 1000 ppm NH_4^+) was diluted sequentially with DI water to produce standard solutions with NH_4^+ concentrations of 100 ppm (pH 6.7), 10 ppm (pH 6.6), 1 ppm (pH 6.7), 0.5 ppm (pH 6.8) and 0.1 ppm (pH 6.9). Calibration of the system was performed at constant room temperature (20.7 °C) in an NH_4^+ concentration range of 0.1−1000 ppm, starting with the lowest concentration. The measured electrical potential ΔV was plotted against the logarithm of the NH_4^+ concentration in solution, giving a linear calibration function (Supporting Information, Figure 12S).

For sample preparation, a weak anion-exchange cartridge (Strata-X AW, 30 mg, Phenomenex, U.S.A.) was preconditioned with 10 mL of MeOH and 20 mL of DI water. To find out about a potential release of NH_4^+ ions from the preconditioned cartridge, a DI water sample (2 mL) was passed through the cartridge, resulting in a NH_4^+ concentration of <0.1 ppm. Subsequently, the corresponding Cu**1b** sample from the thermal stability study was applied onto the cartridge. Cu**1b** was trapped, whereas NH_4^+ ions were released from the anionic complex. The sample eluate was collected, and the NH_4^+ ion content quantified at constant room temperature (20.7 °C) using the NH_4^+ ion-selective electrode.

Chemistry. *[{(2S)-2-(4-aminobenzyl)-1,4,7-triazacyclododecane-N,N′,N″-triyl}triacetate]cuprate(1-) (Cu**1**).* Chelator **1** (18.34 mg, 33.1 μmol) in (500 μL) 0.5 M NH_4OAc buffer (pH 6.8) was added to (340 μL) 0.1 M $CuCl_2$ (34 μmol) in 0.5 M NH_4OAc buffer. The mixture was heated at 90 °C for 20 min. The resulting isomers Cu**1a** and Cu**1b** were fractionized by HPLC system B(II), concentrated by evaporation, and lyophilized. For ESI-MS measurements, Cu**1a** and Cu**1b** were dissolved in DI water, and mass spectra were collected in the negative ion mode (Supporting Information, Figures 1S and 2S). For NMR analysis, a Cu**1b** sample was dissolved in D_2O. For UV−vis and CD spectroscopy, aqueous solutions of Cu**1a** and Cu**1b** were prepared as described in the respective section.

For the Cu-complexation in the subnanomolar range, (0.5 μL) 20 mM chelator **1** (10 nmol) and (0.5 μL) 1 mM $CuCl_2$ (0.5 nmol) were added to 200 μL of HCl (0.04 M) and 299 μL of NH_4OAc buffer (0.5 M). Four mixtures (pH 6.1) were heated at 90 °C for 20 min. Formation of the resulting isomers Cu**1a** and Cu**1b** were subsequently quantified by HPLC system A(II).

ESI-MS: Cu**1a**: *m/z*: 468.4 $[M]^-$, Cu**1b**: *m/z*: 468.1 $[M]^-$. HPLC: A(II): R_T(**1**) 6.3 min, R_T(Cu**1a**) 11.4 min, R_T(Cu**1b**) 16.8 min; A(III): R_T(**1**) 15.2 min, R_T(Cu**1a**) 19.7 min, R_T(Cu**1b**) 28.7 min; B(II): R_T(Cu**1a**) 13.2 min, R_T(Cu**1b**) 17.2 min. UV−vis: λ_{max} (ε): Cu**1a**: 237 nm (7520 M^{-1} cm^{-1}) and 760 nm (64 M^{-1} cm^{-1}), Cu**1b**: 237 nm (7340 M^{-1} cm^{-1}) and 736 nm (53 M^{-1} cm^{-1}).

*[{(2S)-2-(4-aminobenzyl)-1,4,7-triazacyclododecane-N,N′,N″-triyl}-triacetate]nitrate(1-) (Ni**1**).* Chelator **1** (0.55 mg, 1 μmol) in (600 μL) 0.5 M NH_4OAc buffer (pH 7.0) was added to (100 μL) 10 mM $NiNO_3$ (1 μmol) in water. The mixture (pH 6.2) was heated at 90 °C for 20 min. The two isomer species Ni**1a** and Ni**1b** of the [Ni((*S*)-*p*-NH_2-Bn-NOTA)]$^-$ complex were fractionized by HPLC system B(I), concentrated by evaporation, and lyophilized. The complex isomers Ni**1a** and Ni**1b** (each 0.4 mg, 0.9 μmol) were separately dissolved in deionized water, and mass spectra were collected in the negative ion mode.

ESI-MS: Ni**1a**: *m/z*: 463.1 $[M]^-$, Ni**1b**: *m/z*: 463.0 $[M]^-$. HPLC: A(II): R_T(Ni**1a**) 9.7 min, R_T(Ni**1b**) 15.1 min; A(III): R_T(Ni**1a**) 16.3 min, R_T(Ni**1b**) 25.4 min; B(I): R_T(Cu**1a**) 11.9 min, R_T(Cu**1b**) 16.0 min.

Sample Preparation for Thermal Stability Studies. HPLC fractions of Cu**1a** and Cu**1b** in mobile phase (II) (50 mM NH_4OAc buffer, pH 6.0, containing 5% CH_3CN) were used without further processing (method *a*) or prepared as follows: Aliquots of Cu**1a** and Cu**1b** (∼0.1 μmol) were evaporated at 0.160 mbar and 30 °C for 30 min to remove CH_3CN. Subsequently, different freeze-drying procedures were applied to remove NH_4^+ ions from the Cu**1** complexes: the samples were lyophilized at 0.160 mbar and 5 °C for 24 h (method *b*), dissolved in 500 μL of DI water and lyophilized again: at 0.160 mbar and 5 °C for 24 h (method *c*) or at 0.160 mbar and 25 °C for 48 h (method *d*). Finally, all samples were dissolved in 500 μL of DI water.

Thermal Stability Studies. Samples (500 μL) of pure Cu**1a** (0.02−0.43 μmol) and pure Cu**1b** (0.03−0.17 μmol) in NH_4OAc buffer (sample preparation method *a*) and in DI water (sample preparation method *b*-*d*) were incubated at 90 °C in 1.5 mL PP tubes for a total of 500 h. The caps were isolated with aluminum foil to prevent condensation of liquid. At specific time points (0, 24, 72, 142, 238, 287, 332, 407, and 500 h), the samples were cooled down by short centrifugation and a short vigorous mixing. Subsequently, aliquots (30 μL) were sampled into new 1.5 mL PP tubes and kept at −18 °C until analyzed. The aliquots were analyzed with HPLC system A(II) at room temperature by injecting 25 μL of each sample. To study the effect of temperature on the interconversion energy barrier, aliquots (200 μL) of Cu**1a** (1.4 μmol) and Cu**1b** (0.61 μmol) in DI water (method *d*) were incubated separately at 20, 40, 60, 70, 80, 90, and 95 °C for a total of 24 h. The samples were analyzed with HPLC system A(II) at room temperature. The injection volume of each sample was 40 μL.

Calculations. The thermal stability of Cu**1a** (isomer a) and Cu**1b** (isomer b) within 500 h reaction time at 90 °C (Supporting Information, Tables 3S−5S) was calculated using the following equations:

$$\mathrm{Cu\mathbf{1a}}(t_{i,a}) = \frac{A_a + A_b}{A_{0,a}} \quad (1)$$

and

$$\mathrm{Cu\mathbf{1b}}(t_{i,b}) = \frac{A_a + A_b}{A_{0,b}} \quad (2)$$

where t_i is the specific time point of the reaction mixture sampling ($t_{i,a}$ or $t_{i,b}$), A is the UV peak area of the corresponding isomer at the time $t = 0$ ($A_{0,a}$ or $A_{0,b}$) and at the time $t = t_i$ (A_a or A_b).

The determination of the rate constant, energy barrier, and kinetic activation parameters of interconverting enantiomers was previously reviewed in detail by Krupcik et al.[10] Accordingly, the rate constants $k_{a\rightarrow b}$ and $k_{b\rightarrow a}$ of the conformation change of Cu**1a** and Cu**1b** at the

specific times and temperatures were determined by three independent experiments using the rate equation:

$$-\frac{dA_a}{dt} = k_{a\rightarrow b}A_a \quad (3)$$

and

$$-\frac{dA_b}{dt} = k_{b\rightarrow a}A_b \quad (4)$$

where A is the UV peak area of the corresponding isomer and t the reaction time (Supporting Information, Tables 3S−5S). Assuming that the conformation change of the Cu**1** complex is a first order rate reaction, the rate constants $k_{a\rightarrow b}$ and $k_{b\rightarrow a}$ were calculated by integration and modification of the equation:

$$k_{a\rightarrow b} = \frac{1}{t_{i,a}}\ln\frac{A_{0,a}}{A_a} \quad (5)$$

and

$$k_{b\rightarrow a} = \frac{1}{t_{i,b}}\ln\frac{A_{0,b}}{A_b} \quad (6)$$

where t_i is the specific time point of the reaction mixture sampling ($t_{i,a}$ or $t_{i,b}$), A is the UV peak area of the corresponding isomer at time $t = 0$ ($A_{0,a}$ or $A_{0,b}$) and at time $t = t_i$ (A_a or A_b). The free energy barrier of the conformation change of Cu**1a** ($\Delta G_{a\rightarrow b}$) and Cu**1b** ($\Delta G_{b\rightarrow a}$) at the specific time and temperature was calculated using the Eyring equation:

$$-\Delta G_{a\rightarrow b} = RT\ln\left(\frac{hk_{a\rightarrow b}}{\kappa k_B T}\right) \quad (7)$$

and

$$-\Delta G_{b\rightarrow a} = RT\ln\left(\frac{hk_{b\rightarrow a}}{\kappa k_B T}\right) \quad (8)$$

where R is the universal gas constant, T the temperature in K, h is the Planck constant, $k_{a\rightarrow b}$ and $k_{b\rightarrow a}$ are the rate constants of interconversion, κ the transmission coefficient, and k_B the Boltzmann constant. A transmission coefficient $\kappa = 1$ was used for the calculation of the interconversion energy barrier in the Eyring equation.

The activation parameters ($\Delta H_{a\rightarrow b}$, $\Delta H_{b\rightarrow a}$ and $\Delta S_{a\rightarrow b}$, $\Delta S_{b\rightarrow a}$) of the interconversion were calculated using the rate constants ($k_{a\rightarrow b}$ and $k_{b\rightarrow a}$), which were determined at 20, 40, 60, 70, 80, 90, and 95 °C each in four independent experiments. By performing an Arrhenius plot ($\ln(k)$ vs $1/T$), using the uncertainties as weights, a linear relation between $\ln(k)$ and the reaction temperature T was found for both isomers ($r^2 = 0.998$ and 0.986, see Figure 8). The slope of this linear function ($= -E_a/R$) gave the energy of activation (E_a), which was used to determine the activation enthalpies ($\Delta H_{a\rightarrow b}$, $\Delta H_{b\rightarrow a}$) at 37 °C (310 K) using the equation:

$$\Delta H_{a\rightarrow b} = E_{aa\rightarrow b} - RT \quad (9)$$

and

$$\Delta H_{b\rightarrow a} = E_{ab\rightarrow a} - RT \quad (10)$$

Using $\Delta G_{a\rightarrow b}$ and $\Delta G_{b\rightarrow a}$, which were calculated for 37 °C (310 K), the entropies ($\Delta S_{a\rightarrow b}$, $\Delta S_{b\rightarrow a}$) were obtained with the Gibbs−Helmholtz equation:

$$\Delta S_{a\rightarrow b} = \frac{\Delta H_{a\rightarrow b} - \Delta G_{a\rightarrow b}}{T} \quad (11)$$

and

$$\Delta S_{b\rightarrow a} = \frac{\Delta H_{b\rightarrow a} - \Delta G_{b\rightarrow a}}{T} \quad (12)$$

Radiochemistry. *[{(2S)-2-(4-aminobenzyl)-1,4,7-triazacyclododecane-N,N′,N″-triyl}triacetate][^{64}Cu]cuprate(1-) ([^{64}Cu]**1**).* [^{64}Cu]$CuCl_2$ (474 MBq, ESA: 500 GBq/μmol) in 0.04 M HCl (200 μL) and chelator **1** (110 μg, 0.2 μmol) in 2 μL of water were mixed in 0.5 M NH_4OAc buffer solution (200 μL, pH 6.1). The mixture was incubated at 90 °C for 20 min. Subsequently, a saturated aqueous solution of DTPA (5 μL) was added to the reaction mixture to complex nonreacted [^{64}Cu]Cu^{2+}. The complex isomers [^{64}Cu]**1a** and [^{64}Cu]**1b** were separated by HPLC system A(II).

To study the influence of the reaction temperature (T) on the isomer ratio of [^{64}Cu]**1a** to [^{64}Cu]**1b**, four independent experiments were performed for each isomer. [^{64}Cu]$CuCl_2$ (2 MBq, ESA: 3 GBq/μmol) in 0.5 M NH_4OAc buffer (50 μL) and chelator **1** (20 μg, 50 nmol) in 2.5 μL of DI water were mixed in DI water (150 μL). The mixtures (pH 6.2) were heated up to 40 and 99 °C, respectively, for 20 min. Subsequently, a saturated aqueous solution of DTPA (5 μL) was added to the reaction mixture to complex nonreacted [^{64}Cu]Cu^{2+}. The ratios of [^{64}Cu]**1a** to [^{64}Cu]**1b** and Cu**1a** and Cu**1b** were analyzed with HPLC system A(II) by co-evaluation of the UV-trace and the radiometric profile.

To study the influence of the pH on the isomer ratio of [^{64}Cu]**1a** to [^{64}Cu]**1b**, four independent experiments were performed for each isomer at pH 3.5, 5.0, 6.5, and 8.0. [^{64}Cu]$CuCl_2$ (3 MBq, ESA: 33 GBq/μmol) in 0.04 M HCl (10−400 μL) and chelator **1** (20 μg, 50 nmol) in 2.5 μL of DI water were mixed in 0.5 M NH_4OAc buffer solution (200 μL). The mixtures were heated at 90 °C for 20 min. The ratio of [^{64}Cu]**1a** to [^{64}Cu]**1b** was analyzed with HPLC system A(II) by evaluation of the radiometric profile.

To determine the partition coefficients, a 50 mM NH_4OAc buffer solution (pH 6.1) was saturated with 1-octanol in a tube rotator (VWR, Germany) at room temperature overnight. Likewise, 1-octanol was saturated with the NH_4OAc buffer. After HPLC separation of [^{64}Cu]**1a** and [^{64}Cu]**1b** with system A(II), the collected fractions were concentrated in a vacuum concentrator (40 °C, 0.167 mbar, 1 h) to remove the remains of CH_3CN. Six aliquots of [^{64}Cu]**1a** (0.6 MBq, 90 μL) and [^{64}Cu]**1b** (0.7 MBq, 5 μL) were diluted each to 500 μL in the NH_4OAc buffer and, subsequently, overlaid with 500 μL of 1-octanol. All samples were mixed in the tube rotator for 16 h overnight. Thereafter, the phases were separated by centrifugation (3000 *g*, 5 min). A volume of 375 μL was carefully sampled from the upper organic phase, transferred into a new PP tube and again centrifuged (3000 *g*, 5 min). The remaining organic supernatant was discarded. Thereafter, a volume of 300 μL was carefully sampled from the aqueous phase, transferred into a new PP tube, and centrifuged (3000 *g*, 5 min). Aliquots of the aqueous phase (150 μL) and organic phase (300 μL) were transferred separately into VAPEX test tubes (PerkinElmer, U.S.A.). The radioactivity of the organic and aqueous phases was measured in six experiments using the gamma counter 2480 Wizard 3″ (PerkinElmer, U.S.A.). The results were averaged. The log$D_{6.1}$ values of [^{64}Cu]**1a** and [^{64}Cu]**1b** were defined as the ratio of the amount of radiotracer in the organic layer (1-octanol) to that in the aqueous phase:

$$\log D = \log\left(\frac{\text{Activity in organic phase}}{\text{Activity in aqueous phase}}\right) \quad (13)$$

Partition coefficient: log $D_{6.1}$ ([^{64}Cu]**1a**), −3.81 ± 0.08; log $D_{6.1}$ ([^{64}Cu]**1b**), −3.32 ± 0.04. HPLC: A(II): R_T(Cu**1b**) 34.4 min, R_T([^{64}Cu]**1b**) 34.7 min. TLC: R_f([^{64}Cu]**1**) 0.53.

RESULTS

Complex Formation and Characterization. *Formation of the [Cu((S)-p-NH_2-Bn-NOTA)]$^-$ Complex.* After the complexation of Cu^{2+} with the (*S*)-*p*-NH_2-Bn-NOTA **1** chelator, two isomers of the [Cu((*S*)-*p*-NH_2-Bn-NOTA)]$^-$ complex (Cu**1**) were separated by ion pair chromatography. The ratio of Cu**1a** to

dx.doi.org/10.1021/ic101775q |*Inorg. Chem.* 2011, 50, 4260–4271

Table 1. Influence of the Reaction Temperature (T), pH, and Stoichiometry on the Isomer Ratio[a]

	reaction parameters		stoichiometry [nmol]			% fraction of isomer	
entry	T [°C]	pH	**1**	^{64}Cu	Cu	[^{64}Cu]**1b**	Cu**1b**
1	40	6.2	50	2×10^{-4} [b]	1	89 ± 0.19	58 ± 2.0
2	90	3.6	50	2×10^{-4} [c]		91 ± 0.48	
3	90	5.1	50	2×10^{-4} [c]		91 ± 0.22	
4	90	6.6	50	2×10^{-4} [c]		90 ± 0.57	
5	90	8.1	50	2×10^{-4} [c]		90 ± 0.16	
6	90	6.0	40−100	$5-7 \times 10^{-2}$ [c]		89 ± 0.85	
7	99	6.2	50	2×10^{-4} [b]	1	89 ± 0.34	46 ± 1.5
8	90	6.1	10	*d*	0.5		57 ± 3.2
9	90	7.0	1000	*d*	1100		78 ± 3.3

[a] The isomer ratio was analyzed with HPLC (system A(II)) after 20 min reaction time (n = 4). [b] Using low ESA of ^{64}Cu. [c] Using high ESA of ^{64}Cu. [d] Labeling experiment with ^{nat}Cu.

Cu**1b** isomer was estimated to be 1:3 (Table 1, entry 9). A good peak resolution of Cu**1a** and Cu**1b** was achieved using the ion pairing reagents NH_4OAc and triethylammonium acetate (TEAA), respectively (Figure 4B and C). Conversely, no separation of Cu**1a** and Cu**1b** was achieved without an ion pairing reagent in the HPLC mobile phase (system A(I)) (Figure 4A). Furthermore, separate injection of both isomers Cu**1a** and Cu**1b** showed a similar UV profile in HPLC system A(I) with two UV peaks and the same retention times (R_{t1} = 2.2 min and R_{t2} = 2.7 min). Using TLC analysis, equal R_f values were found for both isomers Cu**1a** and Cu**1b** (R_f: 0.53). Therefore, TLC was unsuitable for characterizing the isomer formation of the copper complex because of the low resolution of the TLC.

Formation of the [^{64}Cu((S)-p-NH$_2$-Bn-NOTA)]$^-$ Complex. The radiolabeling of chelator **1** with high ESA of ^{64}Cu (500 GBq/μmol) yielded two [^{64}Cu((*S*)-*p*-NH$_2$-Bn-NOTA)]$^-$ complex isomers [^{64}Cu]**1a** and [^{64}Cu]**1b** with a cumulative radiochemical yield of 93% (Figure 3). In the HPLC analyses, coelution of [^{64}Cu]**1a** and [^{64}Cu]**1b** with the nonradioactive isomers Cu**1a** and Cu**1b**, respectively, was observed (Figure 4D). The isomer ratio of [^{64}Cu]**1a** to [^{64}Cu]**1b** was 1:9. The isomer ratio found under radiochemical conditions thus differed notably from the isomer ratio found after the Cu-complexation under chemical conditions. Additional radiolabeling experiments were therefore performed and analyzed with radio-HPLC, to study the influence of the reaction temperature, the pH, and the stoichiometry of ^{64}Cu to chelator **1** on the isomer ratio (Table 1, entries 1−7). These parameters did not influence the 1:9 ratio at which [^{64}Cu]**1a** and [^{64}Cu]**1b** was formed. Using ^{64}Cu of low ESA for the radiolabeling experiments (Table 1, entry 1 and 7), a strikingly different isomer ratio was, however, observed for the Cu**1a** to Cu**1b** ratio, when co-evaluating the UV profile in the HPLC analyses. While [^{64}Cu]**1a** and [^{64}Cu]**1b** were formed at a ratio of 1:9, an approximate 1:1 ratio was determined for Cu**1a** to Cu**1b**. To verify this observation, additional experiments were performed using an excess of chelator **1** and Cu^{2+} in the subnanomolar concentration range. As a result, an approximate 1:1 ratio was also determined in the HPLC analyses for Cu**1a** to Cu**1b** ((Table 1, entry 8 and Supporting Information, Figure 8S).

The partition coefficients of [^{64}Cu]**1a** and [^{64}Cu]**1b** were determined in the presence of the ion-pairing agent NH_4OAc. The minor isomer [^{64}Cu]**1a** exhibited lower lipophilicity (log$D_{6.1}$: −3.81 (±0.08)) and, as a result, eluted earlier from the reversed phase HPLC column (Figure 4), whereas the major isomer [^{64}Cu]**1b** had a higher lipophilicity (log$D_{6.1}$: −3.32 (±0.04)) and eluted later from the HPLC column.

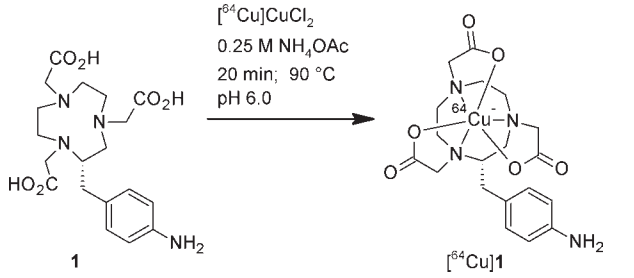

Figure 3. Radiolabeling of the (*S*)-*p*-NH$_2$-Bn-NOTA chelator (**1**) with [^{64}Cu]Cu^{2+}.

Structural Analyses. The complex isomers Cu**1a** and Cu**1b** were analyzed by mass spectrometry, NMR, CD, and UV−vis spectroscopy to obtain information about their structural differences. With mass spectrometry, identical mass spectra for Cu**1a** and Cu**1b** in aqueous solutions were obtained in the negative ion mode. The spectra were showing the characteristic natural isotopic distribution pattern of Cu (^{63}Cu: 69.2%, ^{65}Cu: 30.8%) (Supporting Information, Figure 1S and Figure 2S). The determined molecule mass of the separated isomers Cu**1a** (468.1 [M]$^-$ (69%), 470.1 [M]$^-$ (31%)) and Cu**1b** (468.4 [M]$^-$ (69%), 470.4 [M]$^-$ (31%)) correlated very well with the calculated average mass of the anionic copper complex (469.4 [M]$^-$).

In the NMR analysis, the unpaired electron of Cu(II) caused a strong broadening of the proton NMR signals of Cu**1b** because of the paramagnetic Cu(II) complex (d9 species) (^{1}H−^{1}H COSY spectra in Supporting Information, Figure 5S). Therefore, NMR was unsuitable for further characterizations.

UV−vis spectroscopy was performed on aqueous Cu**1a** and Cu**1b** solutions at wavelengths 190−700 nm and at 500−900 nm. In the UV range a local absorption maximum at 237 nm was found for both isomers with an average extinction coefficient of 7400 M^{-1} cm^{-1}. Within the 500−900 nm range, strikingly different absorption maxima were observed for the two isomers, with peaks located at 760 nm for Cu**1a** and 736 nm for Cu**1b** (Figure 5B). Corresponding extinction coefficients for Cu**1a** and Cu**1b** were 64 and 53 M^{-1} cm^{-1} at their respective λ_{max} values of 760 and 736 nm.

dx.doi.org/10.1021/ic101775q |*Inorg. Chem.* 2011, 50, 4260–4271

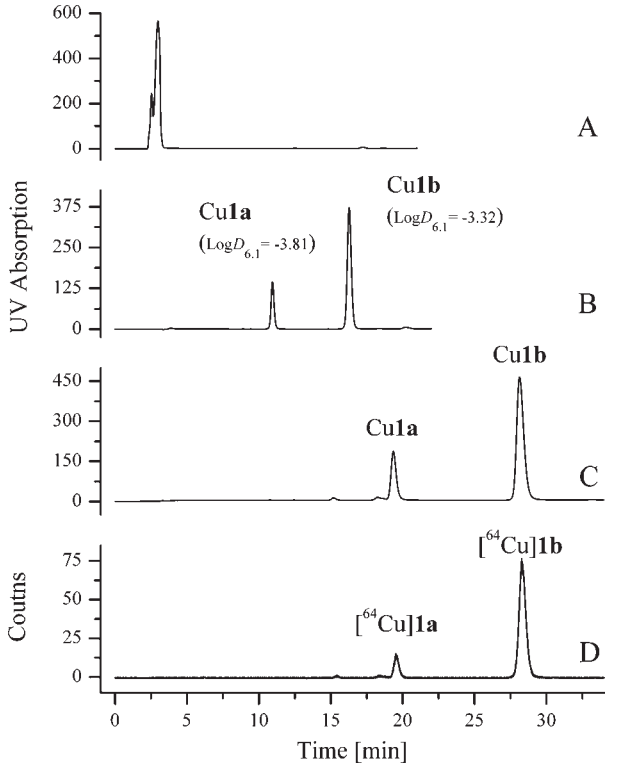

Figure 4. HPLC analysis of a crude reaction mixture of the [Cu((*S*)-*p*-NH_2-Bn-NOTA)]$^-$ complex with different HPLC systems. (A) No separation of complex isomers was achieved with an aqueous solution of 5% CH_3CN as mobile phase (system A(I)). Good separation of complex isomers was achieved with a mixture of 5% CH_3CN and 50 mM NH_4OAc (B) or 50 mM TEAA (C) as mobile phase (system A(II) and A(III)). The isomers Cu**1a** and Cu**1b** formed at a ratio of 1:3. By analyzing a crude reaction mixture of [^{64}Cu((*S*)-*p*-NH_2-Bn-NOTA)]$^-$, the ratio of [^{64}Cu]**1a** to [^{64}Cu]**1b** was 1:9 in the radiometric profile (D).

Using CD spectroscopy measurements, no additional structural information for Cu**1a** and Cu**1b** could be obtained because of the very low signal of the copper complex samples. A kind of fine structure could be detected from both isomers Cu**1a** and Cu**1b** in the middle and far UV region, respectively (Figure 5C). As a demonstration of the fine structure related to the absorption of the samples, the CD spectra were plotted together with absorption spectra (Figure 5A and C). Some of the fine structures followed the structure of the UV−vis absorption spectrum of the samples. In addition, Cu**1a** shows a broader negative signal around 265 nm, and for both isomers a positive signal was obtained at around 207 nm. The far-UV signal of Cu**1a** had a negative tendency, whereas the Cu**1b** signal appeared slightly positive.

Interconversion Studies. The interconversion and thermal stability of Cu**1a** and Cu**1b** was studied in aqueous solution in the presence of the ion pairing reagent NH_4OAc. Since NH_4^+ acts as counterion for the negatively charged copper complex, differences in the thermal stability of Cu**1** most likely depend on the NH_4^+ ion concentration in solution. On this account, the thermal stability of Cu**1a** and Cu**1b** was determined in 50 mM NH_4OAc buffer (method *a*) as well as in DI water (method *b*-*d*) in the presence of different residual contents of NH_4^+ ions (Table 2). For the preparation of "ammonium-free" samples, different freeze-drying procedures were applied to remove NH_4^+ ions from the copper complex. NH_4^+ ions were most efficiently removed by a second lyophilization of the aqueous samples and by increasing the lyophilization temperature from 5 to 25 °C. In this way, the ratio of NH_4^+ to the isomer Cu**1a** could be reduced from 2:1 to approximately 1:3. (Table 2).

The interconversion and thermal stability of the minor isomer Cu**1a** was initially determined in DI water at the lowest NH_4^+ to Cu**1a** ratio of 1:3 (method *d*). The aqueous Cu**1a** solution was heated at 90 °C for a total of 500 h. By analyzing aliquots of the mixture during the reaction time, a conversion of Cu**1a** into the major isomer Cu**1b** was observed (Figure 6B and C). Moreover, the total UV peak area of both isomers Cu**1a** and Cu**1b** decreased over time, indicating a stepwise degradation of the copper complex in solution until complete decomposition after 500 h reaction time (Figure 6D).

Effect of NH_4^+ Ions on the Interconversion Rate Constant. To study the effect of NH_4^+ ions on the interconversion rate constant *k*, samples of pure Cu**1a** and pure Cu**1b** were heated at 90 °C for a total of 24 h in 50 mM NH_4OAc buffer (method *a*, pH 6.0) and in DI water (method *b*−*d*, pH ∼5). The NH_4^+ ion concentration in the samples was determined with an NH_4^+ ion-selective electrode. After 24 h, the interconversion of both isomers Cu**1a** and Cu**1b** was quantified by HPLC analysis, and the rate constants $k_{a\rightarrow b}$ and $k_{b\rightarrow a}$ were calculated using eq 5 and 6, respectively.

As a result, both isomers Cu**1a** and Cu**1b** interconverted at 90 °C. Depending on the NH_4^+ concentration in solution, interconversion rate constants ranging between 5.4×10^{-8} s^{-1} and 1.4×10^{-5} s^{-1} were measured. Generally, a lower NH_4^+ concentration resulted in faster rate constants (Table 2). In addition, the minor isomer Cu**1a** converted faster than the major isomer Cu**1b**.

Long-Term Interconversion Studies. Interconversion of both isomers Cu**1a** and Cu**1b** was observed during a reaction time of 500 h. In general, the minor isomer Cu**1a** converted faster than the major isomer Cu**1b**. Furthermore, both isomers converted faster at low NH_4^+ ion concentrations. The relationship between the Cu**1b** to Cu**1a** ratio and the interconversion time *t* was linear in NH_4OAc buffer and sigmoid in DI water (see Figure 7A and B). At the lowest NH_4^+ concentration (method *d*), the interconversion of Cu**1a** and Cu**1b** reached equilibrium at 70 and 330 h respectively. In this state, both isomers Cu**1a** and Cu**1b** were formed at a ratio of 6:94. In contrast, equilibrium was not attained within 500 h, when pure Cu**1a** was heated at 90 °C in NH_4OAc buffer (method *a*), or in DI water (method *c*) (Figure 7B). Differences between the solvent systems appeared also in terms of the decomposition rate of the copper complex. Whereas more than 40% of Cu**1a** and Cu**1b** were found to be intact in NH_4OAc buffer at 500 h, less than 10% of the complex isomers were detected in DI water (method *c*) at the same time point (Figure 7C and D). For the lowest NH_4^+ concentration (method *d*), complete decomposition of the copper complex was observed already after 400 h.

Calculation of the Interconversion Energy Barrier. The results obtained from the interconversion experiments in NH_4OAc buffer (method *a*) and in DI water (method *c* and *d*) are listed in Tables 3, 4, and 5. Depending on the NH_4^+ ion concentration in solution, the calculated Gibbs free energy barriers of the conformational change of the complex isomers Cu**1a** and Cu**1b** ranged between 122 kJ mol^{-1} and 141 kJ mol^{-1}.

Determination of Activation Parameters. The dependence of the interconversion free energy barrier ($\Delta G_{a\rightarrow b}$, $\Delta G_{b\rightarrow a}$) on temperature was used to determine the activation enthalpy ($\Delta H_{a\rightarrow b}$, $\Delta H_{b\rightarrow a}$) and activation entropy ($\Delta S_{a\rightarrow b}$, $\Delta S_{b\rightarrow a}$). The rate constant was determined at different temperatures

dx.doi.org/10.1021/ic101775q |*Inorg. Chem.* 2011, 50, 4260–4271

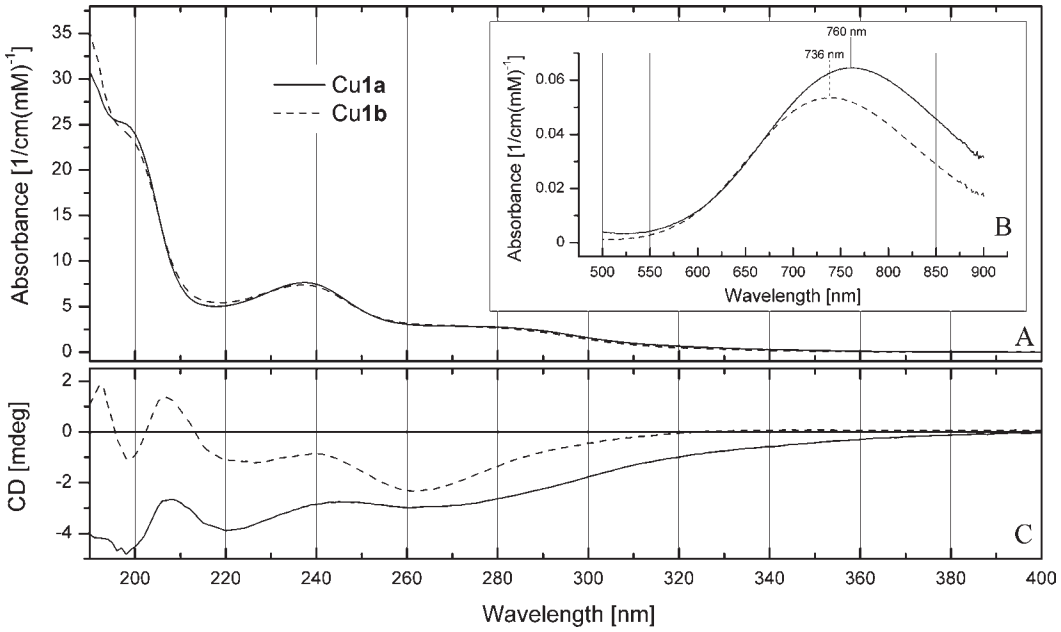

Figure 5. UV−vis and CD absorption spectra of aqueous Cu**1a** and Cu**1b** solutions. (A and B) UV−vis absorption spectra of Cu**1a** and Cu**1b** in the regions 190−400 nm and 500−900 nm. Overlapping of the UV−vis spectra in the wavelength range 500−700 nm is shown in the Supporting Information, Figure 10S. (C) CD spectra of the aqueous Cu**1a** and Cu**1b** solutions.

Table 2. Effect of NH_4^+ Ions on the Rate Constant $k_{a\rightarrow b}$ and $k_{b\rightarrow a}$[a]

		interconversion of Cu**1a**				interconversion of Cu**1b**			
		conc. [μM]		ratio of	rate const.	conc. [μM]		ratio of	rate const.
entry	Sample (prep. method)	NH_4^+	Cu**1a**	NH_4^+: Cu**1a**	$k_{a\rightarrow b}$ [s^{-1}]	NH_4^+	Cu**1b**	NH_4^+: Cu**1b**	$k_{b\rightarrow a}$ [s^{-1}]
1	*a*	50000	63	790: 1	7.09×10^{-7}	50000	68	730: 1	5.38×10^{-8}
2	*b*	143	63	2: 1	7.88×10^{-7}	172	78	2: 1	6.79×10^{-8}
3	*c*	19	35	1: 1.8	1.91×10^{-6}	18	76	1: 4	1.60×10^{-7}
4	*d*	242	864	1: 3.4	1.42×10^{-5}	27	349	1: 13	2.49×10^{-7}

[a] The NH_4^+ ion concentration in the samples was analyzed using an NH_4^+ ion-selective electrode. The concentration of the corresponding complex isomer was calculated from the corresponding UV chromatogram of the HPLC analysis by using the molar extinction coefficient. HPLC analyses were performed before and after heating the complex isomers at 90 °C for 24 h in (1) 50 mM NH_4OAc buffer solution (sample preparation method *a*) and (2−4) in DI water (sample preparation method *b*−*d*). The pH of the samples was pH 6.0 (method *a*), pH 5.1 (method *b*), pH 5.0 (method *c*), pH 5.0−5.6 (method *d*).

(Table 6). The resulting Arrhenius plots of $\ln(k)$ versus $1/T$ are shown in Figure 8. On the basis of this, the activation parameters were calculated. The activation enthalpy (ΔH) as well as the entropic term $-T\Delta S$ was positive for this interconversion process (Table 7). Both contribute positively to the free activation energy (ΔG) in correspondence to the Gibbs−Helmholtz equation. For both directions of interconversion, the same activation enthalpies were determined at 37 °C ($\Delta H_{a\rightarrow b}$ = 77.64 kJ mol^{-1} and $\Delta H_{b\rightarrow a}$ = 77.68 kJ mol^{-1}). Despite this, the activation entropies of the conformational change were found to be higher for the direction Cu**1a** to Cu**1b** ($\Delta S_{a\rightarrow b}$ = −0.1252 kJ mol^{-1} K^{-1}) and lower for Cu**1b** to Cu**1a** ($\Delta S_{b\rightarrow a}$ = −0.1584 kJ mol^{-1} K^{-1}).

DISCUSSION

Isomer Formation of the [^{64}Cu((*S*)-*p*-NH_2-Bn-NOTA)]$^-$ Complex. The complexation of ^{64}Cu with the chelator **1** leads to the formation of two complex isomers which can be separated using ion pair chromatography (Figure 4). This observation is relevant for the preparation of [^{64}Cu-NOTA-Bn]-labeled radiotracers. During the ^{64}Cu complexation of a (bio)molecule, which is functionalized with chelator **1**, two different compounds form and each complex isomer could influence the in vivo behavior of the labeled (bio)molecule differently. Moreover, the impact of the isomers on conjugated low-molecular weight fragments, which potentially derive from the in vivo metabolism of the radiolabeled (bio)molecule, has to be viewed more critically. Knowledge of the structural differences of the complex isomers, as well as their chemical properties, for example, differences in the complex charge, lipophilicity, or interconversion energy barrier, is important to assess the influence of the complex isomers on the molecule to be labeled. In this study, several analytical methods were utilized to characterize for the first time the separated isomers Cu**1a** and Cu**1b**.

dx.doi.org/10.1021/ic101775q |*Inorg. Chem.* 2011, 50, 4260–4271

The observation that a retention and a good separation of [^{64}Cu]**1a** and [^{64}Cu]**1b** in reversed phase HPLC was achieved in the presence of ion-pairing agents (Figure 4) such as NH_4OAc and TEAA, reveals that both isomers are anionic complexes. This conclusion was supported by ESI-MS analyses of Cu**1a** and Cu**1b**, showing identical spectra for both isomers in the negative ion mode (Supporting Information, Figures 1S and 2S). Because of their negative charge, both isomers Cu**1a** and Cu**1b** retarded completely on a weak anion exchange resin and eluted after the addition of a TFA solution (Supporting Information, Figure 7S). Therefore, the anion exchange resin was used for the interconversion studies to quantify the release of NH_4^+ ions, which were probably bound to the complex in the form of a second-sphere NH_3-adduct.

[^{64}Cu]**1a** exhibited lower lipophilicity (log$D_{6.1}$: −3.81 (±0.08)) than [^{64}Cu]**1b** (log$D_{6.1}$: −3.32 (±0.04)). This could lead to differences in the biodistribution profile of the isomers, as also suggested by a previous study, where differences in the lipophilicity of two [^{86}Y((*S*)-*p*-NH_2-Bn-DOTA)]$^-$ complex isomers affected the biodistribution in Wistar rats, resulting in a higher liver uptake of the more lipophilic isomer.[11]

An additional aspect of the isomerism of the [^{64}Cu((*S*)-*p*-NH_2-Bn-NOTA)]$^-$ complex is the [^{64}Cu]**1a** to [^{64}Cu]**1b** ratio after the radiolabeling. Normally, the radiolabeling is performed with an excess of chelator **1** in a buffer solution at pH 3.5 to 8.0 and a reaction temperature between 40 and 99 degrees. Under these conditions the two complex isomers were formed at a ratio of 1:9 (Table 1), and the isomer ratio was influenced neither by the reaction temperature nor by the pH in the mentioned range. Also a variation of the radiometal to chelator stoichiometry, using different amounts of ^{64}Cu between 2 MBq and 500 MBq, did not affect the 1:9 isomer ratio. In contrast, a notably different isomer ratio was found under radiochemical conditions for the [^{64}Cu]**1** and the Cu**1** complex in the same solution, after co-evaluating the UV and radiometric profile of the HPLC analyses. While [^{64}Cu]**1b** was the major isomer with a fraction of 90%, the nonradioactive Cu**1a** to Cu**1b** ratio was approximately equal. Moreover, the equimolar Cu**1a** to Cu**1b** ratio, which was found under radiochemical conditions, is a finding contrary to the 78% Cu**1b** fraction, which was found under chemical conditions, using micromolar amounts of Cu^{2+} and **1** in equal stoichiometry. Thus far, we are unable to give a detailed explanation for the observed variance in the isomer formation of the Cu**1** complex.

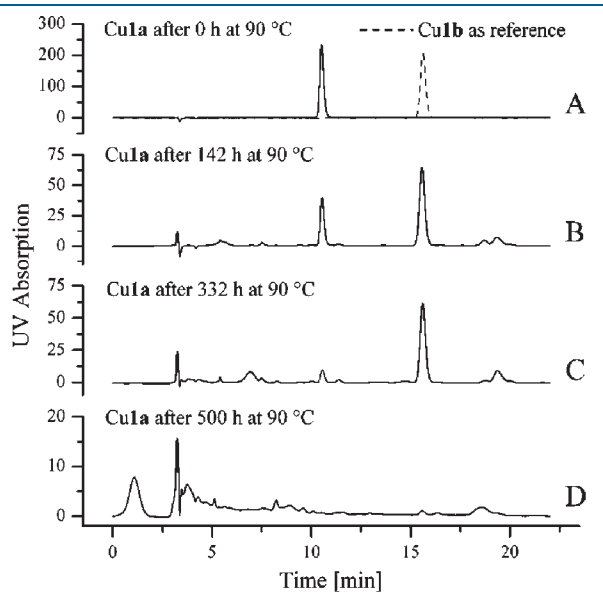

Figure 6. HPLC analyses of a pure Cu**1a** sample after thermal treatment at 90 °C in DI water (sample preparation method *d*). (A) Overlay of the UV profiles of Cu**1b** as reference and the Cu**1a** sample before thermal treatment. (B−D) UV profiles of the Cu**1a** sample after 142, 336, and 500 h heating to 90 °C.

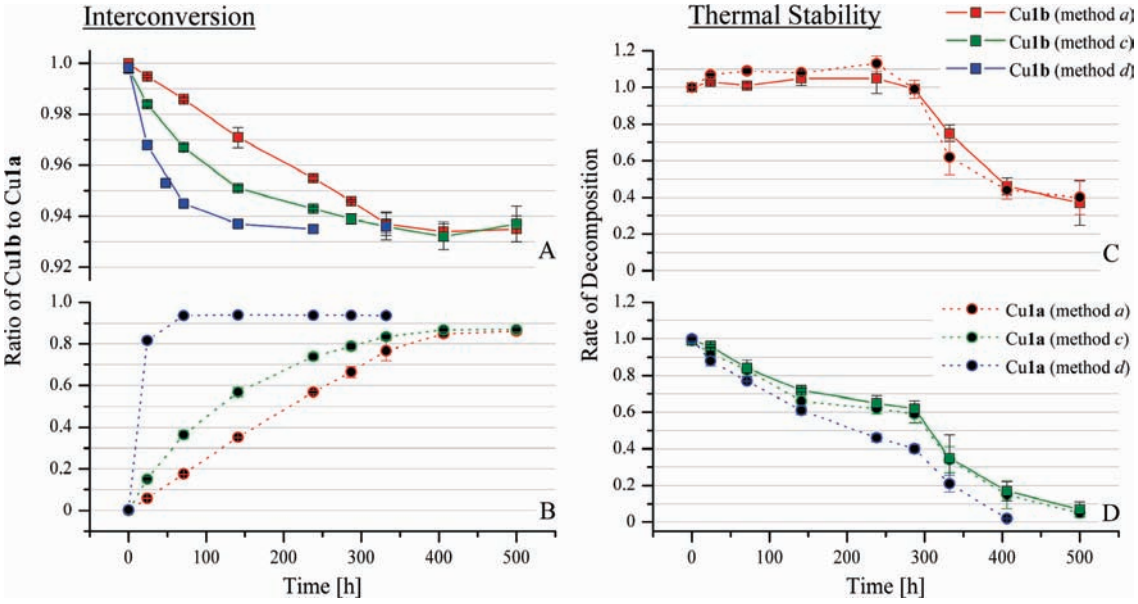

Figure 7. HPLC analyses of the interconversion and thermal stability of pure Cu**1a** and pure Cu**1b** isomer at 90 °C in 50 mM NH_4OAc buffer solution (method *a*) and in DI water (method *c, d*) at given time points ($n = 3$). (A, B) Relationship between the isomer ratios, found for Cu**1a** (A) and Cu**1b** (B), and the reaction time. (C, D) Relationship between the decomposition of the complex isomers, found in 50 mM NH_4OAc solution (C) and DI water (D), and the reaction time.

dx.doi.org/10.1021/ic101775q |*Inorg. Chem.* 2011, 50, 4260–4271

Table 3. Rate Constants and Gibbs Free Energy Barriers of the Interconversion of Pure Cu1a and Cu1b in 50 mM NH_4OAc Buffer Solution (Method *a*) at 90 °C

	rate constant [s^{-1}]		free energy barrier [kJ mol^{-1}]	
time [h]	$k_{a\rightarrow b}$	$k_{b\rightarrow a}$	$\Delta G_{a\rightarrow b}$	$\Delta G_{b\rightarrow a}$
24	7.09×10^{-7}	5.38×10^{-8}	132.3	140.1
71	7.48×10^{-7}	5.42×10^{-8}	132.1	140.1
141	8.46×10^{-7}	5.77×10^{-8}	131.8	139.9
238	9.79×10^{-7}	5.32×10^{-8}	131.3	140.1
287	1.06×10^{-6}	5.35×10^{-8}	131.1	140.1
332	1.22×10^{-6}	5.41×10^{-8}	130.7	140.1
406	1.29×10^{-6}	4.63×10^{-8}	130.5	140.5
500	1.10×10^{-6}	3.76×10^{-8}	131.0	141.2

Table 4. Rate Constants and Gibbs Free Energy Barriers of the Interconversion of Pure Cu1a and Cu1b in DI Water (Method *c*) at 90 °C

	rate constant [s^{-1}]		free energy barrier [kJ mol-1]	
time [h]	$k_{a\rightarrow b}$	$k_{b\rightarrow a}$	$\Delta G_{a\rightarrow b}$	$\Delta G_{b\rightarrow a}$
24	1.91×10^{-6}	1.82×10^{-7}	129.3	136.4
71	1.75×10^{-6}	1.28×10^{-7}	129.6	137.5
141	1.64×10^{-6}	9.80×10^{-8}	129.8	138.3
238	1.57×10^{-6}	6.87×10^{-8}	129.9	139.3
287	1.50×10^{-6}	5.96×10^{-8}	130.0	139.8
332	1.49×10^{-6}	5.43×10^{-8}	130.0	140.1
406	1.37×10^{-6}	4.59×10^{-8}	130.3	140.6
500	1.15×10^{-6}	3.71×10^{-8}	130.8	141.2

Table 5. Rate Constants and Gibbs Free Energy Barriers of the Interconversion of Pure Cu1a and Cu1b in DI Water (Method *d*) at 90 °C

	rate constant [s^{-1}]		free energy barrier [kJ mol^{-1}]	
time [h]	$k_{a\rightarrow b}$	$k_{b\rightarrow a}$	$\Delta G_{a\rightarrow b}$	$\Delta G_{b\rightarrow a}$
24	1.97×10^{-5}	3.77×10^{-7}	122.3	134.2
71	e.s.[a]	2.79×10^{-7}	e.s.[a]	135.1
141	e.s.[a]	2.17×10^{-7}	e.s.[a]	135.9

[a] Equilibrium was reached.

Nonetheless, the results suggest that the isomer ratio may be affected by the stoichiometry of metal and chelator.

Interconversion Studies. An important observation was made during the thermal treatment of the separated complex isomers Cu**1a** and Cu**1b**. Both complex isomers interconverted over a time period of several days (Figure 7). Furthermore, differences were observed for both isomers in their interconversion kinetics and thermal stability during the thermal treatment in NH_4OAc buffer solution and in DI water, respectively. The observed influence of the buffer system on the interconversion as well as the stability of the isomers can be explained with a stabilization of the anionic copper complex through NH_4^+ ions. Consequently, the interconversion rates of Cu**1a** and Cu**1b** were faster in DI water. The greater instability of the copper complex

Table 6. Rate Constants of the Conformation Change of Cu1a and Cu1b in DI Water at Different Temperatures[a]

	rate constant [s^{-1}]	
temperature [°C]	$k_{a\rightarrow b}$	$k_{b\rightarrow a}$
20	2.271×10^{-8}	2.421×10^{-9}
40	2.239×10^{-7}	2.525×10^{-9}
60	1.360×10^{-6}	2.492×10^{-8}
70	4.077×10^{-6}	
80	4.213×10^{-6}	1.295×10^{-7}
90	1.411×10^{-5}	2.288×10^{-7}
95	1.735×10^{-5}	

[a] The rate constants $k_{a\rightarrow b}$ and $k_{b\rightarrow a}$ were calculated for the interconversion in DI water (method *d*) ($n = 4$). For Cu**1a**, the interconversion was studied also at 70 and 95 °C.

Table 7. Activation Parameters of the Conformation Change of Cu1a and Cu1b in DI Water (Method *d*) at 37 °C (310 K)

parameter	value
$E_{a,\ a\rightarrow b}$ [kJ mol^{-1}]	80.22
$E_{a,\ b\rightarrow a}$ [kJ mol^{-1}]	80.26
$\Delta G_{a\rightarrow b}$ [kJ mol^{-1}]	116.5
$\Delta G_{b\rightarrow a}$ [kJ mol^{-1}]	126.8
$\Delta H_{a\rightarrow b}$ [kJ mol^{-1}]	77.64
$\Delta H_{b\rightarrow a}$ [kJ mol^{-1}]	77.68
$\Delta S_{a\rightarrow b}$ [kJ mol^{-1} K^{-1}]	−0.1252
$\Delta S_{b\rightarrow a}$ [kJ mol^{-1} K^{-1}]	−0.1584
$-T\Delta S_{a\rightarrow b}$ [kJ mol^{-1}]	38.81
$-T\Delta S_{b\rightarrow a}$ [kJ mol^{-1}]	49.10

in DI water may be caused by a lack of shielding by NH_4^+ ions that results in faster hydrolysis and interconversion of the complex isomers Cu**1a** and Cu**1b**. On this account, we propose that NH_4^+ ions inhibit the interconversion process of the copper complex. This observation is contrary to the findings made in ref 12, where ammonium ions were found to catalyze the interconversion of a cyclam-Cu(II) system. With regard to ref 12 also another, so far unknown explanation can account for the higher stability of the copper complex Cu**1** in solution of ammonium acetate.

Depending on the NH_4^+ ion concentration in solution, the interconversion free energy barrier ΔG of Cu**1a** and Cu**1b** ranged between 122 kJ mol^{-1} and 141 kJ mol^{-1} (Table 3−5). Generally, lower ΔG values were found for lower NH_4^+ concentration, which confirms the assumption that the interconversion is inhibited by NH_4^+ ions. Furthermore, a comparison between Cu**1a** and Cu**1b** demonstrated higher ΔG values for the conformational change a→b than for b→a. The difference in $\Delta G_{a\rightarrow b}$ and $\Delta G_{b\rightarrow a}$ was approximately 10 kJ mol^{-1} in both NH_4OAc buffer and DI water.

The activation enthalpy (ΔH) as well as the entropic term $-T\Delta S$ was positive for this interconversion process (Table 7), and therefore, contributes positively to the free activation energy (ΔG). Since the same activation enthalpies were determined for both directions of interconversion, the observed differences in the free activation energy must originate from differences in the entropy change. A comparison of the results

dx.doi.org/10.1021/ic101775q |*Inorg. Chem.* 2011, 50, 4260–4271

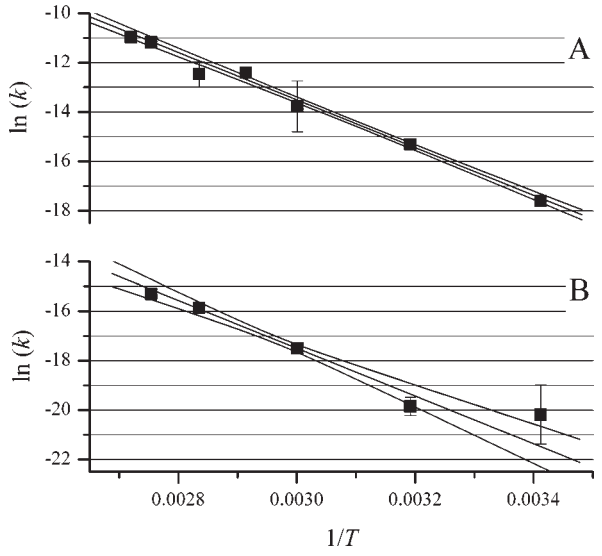

Figure 8. Arrhenius plots ($\ln(k)$ vs $1/T$) of the conformation change of pure Cu**1a** (A) and pure Cu**1b** (B). Plotting and linearization were carried out by using data listed in Table 6 (95% confidence interval) ($n = 4$).

shows that the entropic term $-T\Delta S$ of the conformational change of Cu**1b** (b→a) was approximately 10 kJ mol^{-1} higher at 37 °C. This shows that the entropic energy barrier for Cu**1b** is significantly higher than for Cu**1a**. Thus, we conclude that Cu**1b** is the more stable isomer in terms of thermodynamics and kinetics.

Characterization of the Cu1a and Cu1b Complex Isomers. *Structure of Cu-NOTA Complexes.* The structure of the $[Cu(NOTA)]^-$ complex has been previously examined in solid state and in solution by X-ray crystallography,[13,14] spectrophotometry,[15] and electron paramagnetic resonance (EPR) spectroscopy[16] (Figure 9A). The studies reveal that the coordination behavior of $[Cu(NOTA)]^-$ is complex. An early crystallographic study showed, for example, that $[Cu(NOTA)]^-$ exists as an anionic complex with a six-coordinated CuN_3O_3 polyhedron and a twisted prismatic geometry: an intermediate between an ideal octahedron and a triangular prism.[14] Later, Van der Merwe et al. studied the cationic complex $[CuCl(NOTA)H_2]$ in the solid state.[13] This structure showed a higher level of distortion, resulting from two protonated carboxylate groups which are either weak or not coordinated to the metal center. In addition, the structure of the $[Cu(NOTA)]^-$ complex was pH dependent in solution.[15,16] When the complex is five-coordinated in acidic solutions, through a protonated single carboxylate group, two isomeric species were observed at pH 7, with the ligand being six- and five-coordinated.[16] To give an explanation for the structural difference of Cu**1a** and Cu**1b**, we discuss our results with regard to the previous hypotheses on the occurrence of two isomeric forms of the structural analogue $[Cu(NOTA)]^-$ complex.

*Structure of Cu**1a** and Cu**1b** - Hypothesis A.* By comparing Figure 6A and Figure 6C−D, Cu**1a** indicates to be more stable. It has to convert to Cu**1b** so that its decomposition is possible. As a consequence, Cu**1b** is more labile and decomposes easily. Accepting the known structures of Cu(II) NOTA complexes,[13,14] we can conclude as hypothesis *A* that Cu**1a** is the more stable species and fully coordinated, and Cu**1b** is the less stable species and only two carboxylate groups are coordinated. Accordingly, we found different absorption spectra for both complex isomers in the visible region of 500−900 nm. The spectrum of Cu**1a** exhibits an absorption maximum at 760 nm, whereas the maximum of Cu**1b** is hypsochromically shifted to 736 nm. The corresponding molar extinction coefficients of 64 and 53 M^{-1} cm^{-1} are typical for d-d transitions in Cu(II)-complexes with a tetragonal Jahn−Teller distortion.[16] In accordance with previous spectrophotometric studies,[15] Cu**1a** can be assigned as a six-coordinated $[Cu((S)$-p-NH_2-Bn-NOTA$)]^-$ complex most likely appearing with a trigonal distortion from the idealized octahedral geometry. Thus, protonation of one carboxylate group of Cu**1a** leads to the formation of a five-coordinated $[Cu(H(S)$-p-NH_2-Bn-NOTA$)]$ complex, which can be assigned as Cu**1b**. Notably, the hypsochromical shift from Cu**1a** (760 nm) to Cu**1b** (736 nm) was found to be smaller than the reported shift of $[Cu(NOTA)]^-$ (750 nm) to the protonated $[Cu(HNOTA)]$ complex form (660 nm).[15,16] The smaller difference of λ_{max} for Cu**1a** and Cu**1b** reveals that the release of strain, which we connect with the conversion of Cu**1a** to Cu**1b**, is smaller in comparison with the discussed Cu(II) NOTA system. Moreover, the results indicate that Cu**1b** like Cu**1a** exhibits a high level of distortion in the ligand field.

Despite this assignment, which was basically made on the spectrophotometric data, the proposed model has substantial limitations. Hypothesis *A* contravenes the former statement that Cu**1b** is the more stable isomer in terms of our thermodynamic and kinetic data. Beyond that, if the chelate Cu**1b** is substantially less stable and metal release much more likely, then it would seem possible, but not certain, that the observed interconversion into Cu**1a** occurs through a release of the Cu ion. Furthermore, hypothesis *A* does not account for why only one isomer remains after a considerable period of heating and can not explain the high energy barrier observed for the isomerization.

It is worth mentioning that a Cu(II)-macrocycle isomerism based on a different coordination sphere is exemplified, for example, in ref 12. In this study, two isomers of a cyclam-Cu(II) system have been described as pentacoordinated (conformation I) and hexacoordinated (conformation III) complexes. This result was substantiated by X-ray analysis of the different conformations.

*Structure of Cu**1a** and Cu**1b** - Hypothesis B.* Coordination chemistry of transition metal complexes with azamacrocyclic ligands offers another hypothesis.[17] On one side, the relative orientation of the three carboxylate groups of $[Cu(NOTA)]^-$ is expected to differ in terms of their helicity. A rotation of the carboxylate groups changes the absolute configuration (Δ or Λ) of the complex, as previously demonstrated for metal complexes of DOTA.[17,18] This could lead to the formation of different stereoisomers (Figure 9B). In addition, a conformational change of the azamacrocyclic ring has to be taken into account as another element of chirality. Different arrangements of the CH_2-CH_2 bond are affected by an inversion of the macrocyclic ring. Thereby, two different isomeric ring conformations, ($\delta\delta\delta$) and ($\lambda\lambda\lambda$), are formed (Figure 9C).

Furthermore, the insertion of a substituent onto the carbon framework of the triazamacrocycle introduces a new chiral center leading to the formation of additional stereoisomers. For steric reasons, a bulky substituent locks the complex into a $\delta\delta\delta$-conformation and inhibits a ring flip motion to the $\lambda\lambda\lambda$-conformation (Figure 10), as has been previously observed for two structurally similar complexes, $[Y((S)$-p-NH_2-Bn-DOTA$)]^-$ and $[Ln((S)$-p-NO_2-Bn-DOTA$)]^-$.[11,19] Hence, only the rotation of the acetate arms should take place in the $[Cu((S)$-p-NH_2-Bn-NOTA$)]^-$ complex resulting in a Λ or Δ conformation.

On the basis of this, we propose as hypothesis *B* that the observed isomers of the $[Cu((S)$-p-NH_2-Bn-NOTA$)]^-$ complex

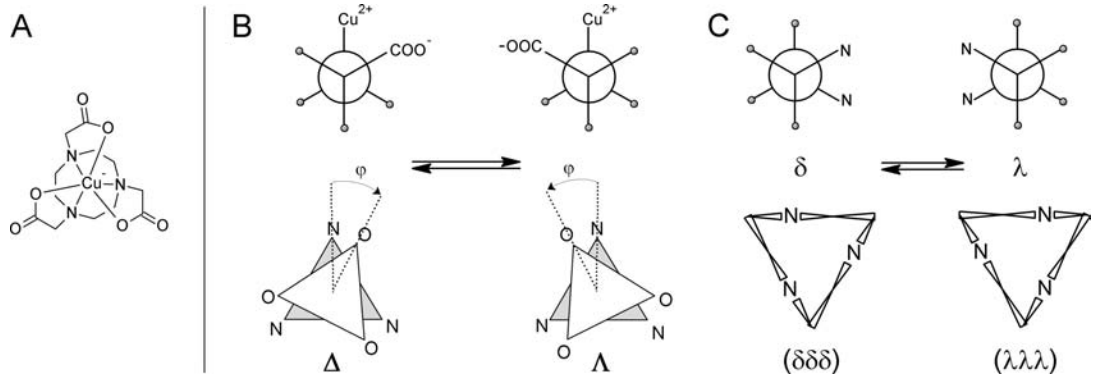

Figure 9. Proposed stereochemistry of the $[Cu(NOTA)]^-$ complex (A). Four possible isomer structures can result from a carboxylate arm rotation and a ring inversion of the azamacrocycle. (B) The Newman projection along the C−N bond of a carboxylate group is depicted, showing the equilibrium between the Δ and Λ chirality of the coordination cage. The triangles show the degree of distortion (twist angle φ) from the regular octahedral arrangement of the N_3O_3 donor set. (C) The Newman projection along an ethylene bond is depicted, showing the equilibrium between the δ and λ chirality of the azamacrocycle. The wedge-type representation of the azamacrocycle in the [333] conformation shows the different isomeric forms in *gauche* projection. The figure has been adapted with permission from ref 18, Copyright 1998 Elsevier.

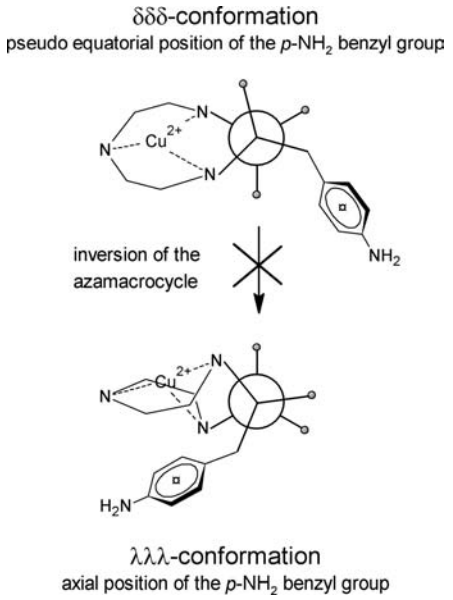

Figure 10. Newman projection of the $[Cu((S)\text{-}p\text{-}NH_2\text{-Bn-NOTA})]^-$ complex Cu**1** along the CH_2-CH-R bond as a model for hypothesis *B*. For steric reasons, the bulky *p*-NH_2 benzyl substituent should adopt the pseudo equatorial conformation to avoid interactions with the macrocycle.

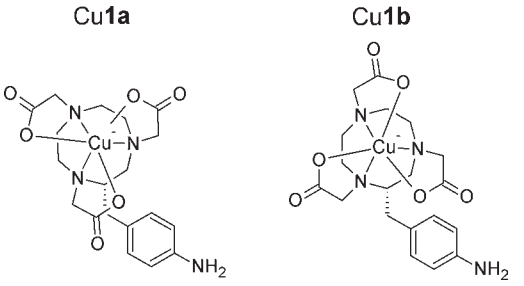

Figure 11. Proposed structures of the two $[Cu((S)\text{-}p\text{-}NH_2\text{-Bn-NOTA})]^-$ complex isomers Cu**1a** and Cu**1b**.

differ in terms of the helicity of their carboxylate groups (Figure 11). As an explanation, we suggest that the interconversion of Cu**1a** and Cu**1b** takes place by a reorientation of the three acetate groups resulting in six-coordinated complexes. A synchronous rotation of the three carboxylate groups in Cu**1** would also explain the high energy barrier of approximately 130−140 kJ mol^{-1} found for both isomers. Interestingly, no interconversion was observed for two $[Y((S)\text{-}p\text{-}NH_2\text{-Bn-DOTA})]^-$ complex conformers during their separate incubation in water for 7 days at 90 °C.[11] This indicates that the interconversion energy barrier of these Y-DOTA conformers is even higher than that of the Cu**1** isomers. An internal reorientation of the acetate groups in Cu**1** is also consistent with the negative activation entropies found for both isomers. In conclusion, in both isomers, internal motion is restricted; however, this restriction seems larger in case of Cu**1b**. This shows also in a narrower negative CD-signal of Cu**1b** and a slightly narrower UV absorption signal around 265 nm (Figure 5). Notably, the activation entropy for the conversion of Cu**1b** to Cu**1a** was found to be more negative ($\Delta S_{b\rightarrow a} = -0.1584$ kJ mol^{-1} K^{-1}) than for the conversion of [Cu(HNOTA)] to the six-coordinated $[Cu(NOTA)]^-$ complex ($\Delta S = -0.054$ kJ mol^{-1} K^{-1}).[14] This might derive from an internal reorientation of the three carboxylate groups, resulting either in a release of strain or in a more effective metal−ligand interaction. Furthermore, we also conclude that the different helicity of Cu**1a** and Cu**1b** influence their electric dipole moments and, therefore, affect the lipophilicity of both isomers as well as their retention times in HPLC (Figure 4). In addition, the results of the mass spectrometry and anion-exchange chromatography of Cu**1a** and Cu**1b** support the conclusion that both isomers are six-coordinated. In this context, it is worth mentioning that the complexation of the six-coordinating Ni(II) ion with chelator **1** also leads to the formation of two anionic complex isomers Ni**1a** and Ni**1b** (Supporting Information, Figures 3S and 4S). This, and the observation that the HPLC profiles of the Cu**1** complex and structural analogue Ni**1** complex (Supporting Information, Figure 9S) are very similar, indicate that Cu**1a** and Cu**1b** are six-coordinated complexes.

However, hypothesis *B* also has its limitations. Without additional data the coordination properties of a DOTA Y(III) ion (8/9-coordination) system cannot be directly compared with those of a NOTA Cu(II) ion (5/6-coordination) system. The analytical data obtained in this study support neither hypothesis

A nor hypothesis *B* exclusively. Unfortunately, our attempts to crystallize the major isomer Cu**1b**, to solve the solid structure, were not successful. Because of this, and because the complex degradation process of the Cu**1** chelate hampers the reaction rate studies, the mechanism of the interconversion remains unclear, and none of the two suggested hypotheses can be verified. Despite the missing evidence for the coordination geometry, a potential impact of the chelate unit [^{64}Cu]**1** on the molecule to be labeled is already demonstrated by the different lipophilicity of [^{64}Cu]**1a** and [^{64}Cu]**1b**. On this account, further investigations should be undertaken to analyze the solid structure of both isomers, as well as to characterize the in vivo behavior of the [^{64}Cu]**1** complex isomers.

CONCLUSION

On the basis of our results, we conclude that different conformational isomer structures of the ^{64}Cu-NOTA complex lead to an isomerization of [^{64}Cu-NOTA-Bn]-labeled radiotracers. Interconversion studies and spectrophotometric measurements with the nonradioactive model complex [Cu((*S*)-*p*-NH_2-Bn-NOTA)]$^-$ (Cu**1**) revealed two isomers adopting different geometrical configurations. The structural difference between the two isomers may be explained either by the presence of penta- and hexa-coordinated complex forms or by the differences in the helicity of the carboxylate side arms (Λ or Δ conformation). As a result, isomer Cu**1a** and Cu**1b** differ in their retention time in HPLC as well as in lipophilicity. For this reason, it is important to characterize the influence of the [^{64}Cu]**1** chelate unit on the in vivo behavior of the (bio)molecule to be labeled.

ASSOCIATED CONTENT

Supporting Information. IEX gradient parameters, CD measurement parameters, ESI-MS spectra of Cu**1a**, Cu**1b**, Ni**1a**, and Ni**1b**, ^{1}H-^{1}H COSY spectrum of Cu**1b**, Elution profiles of **1** and Cu**1**, UV and CD spectra of Cu**1a** and Cu**1b**, HPLC chromatogram of Cu**1** and Ni**1**, calibration curve for the NH_4^+ ion-selective measurement and tables of the normalized UV peak areas and decomposition rates of Cu**1a** and Cu**1b**. This material is available free of charge via the Internet at http://pubs.acs.org.

AUTHOR INFORMATION

Corresponding Author

*E-mail: schlesin@gmx.de. Phone: +358 2 313 3566. Fax: +358 2 213 8191.

ACKNOWLEDGMENT

The study was conducted within the "Centre of Excellence in Molecular Imaging in Cardiovascular and Metabolic Research" supported by the Academy of Finland, University of Turku, Turku University Hospital, and Åbo Akademi University. This work was supported by the EU-FP7 integrated project Beta-Image contract no.: 222980. The authors thank Dr. Francesco Tisato for discussing the coordination chemistry and Dr. Viki-Veikko Elomaa for discussing statistical matters.

ABBREVIATIONS

CD, circular dichroism; DI water, deionized water; DOTA, 1,4,7,10-tetraazacyclododecane-*N*,*N*′,*N*″,*N*‴-tetraacetic acid; DTPA, diethylene triamine pentaacetic acid; ESA, effective specific activity; NOTA, 1,4,7-triazacyclononane-*N*,*N*′,*N*″-triacetic acid; (*S*)-*p*-NH_2-Bn-NOTA, (*S*)-2-(4-Aminobenzyl)-NOTA; TEAA, triethylammonium acetate

REFERENCES

(1) Wadas, T. J.; Wong, E. H.; Weisman, G. R.; Anderson, C. J. *Chem. Rev.* **2010**, *110*, 2858–2902.
(2) Lee, S.; Xie, J.; Chen, X. *Chem. Rev.* **2010**, *110*, 3087–3111.
(3) Anderson, C. J.; Welch, M. J. *Chem Rev* **1999**, *99*, 2219–2234.
(4) Prasanphanich, A. F.; Nanda, P. K.; Rold, T. L.; Ma, L. X.; Lewis, M. R.; Garrison, J. C.; Hoffman, T. J.; Sieckman, G. L.; Figueroa, S. D.; Smith, C. J. *Proc. Natl. Acad. Sci. U.S.A.* **2007**, *104*, 12462–12467.
(5) Liu, Z. F.; Yan, Y. J.; Liu, S. L.; Wang, F.; Chen, X. Y. *Bioconjug. Chem.* **2009**, *20*, 1016–1025.
(6) Kim, Y. S.; Yang, C. T.; Wang, J.; Wang, L.; Li, Z. B.; Chen, X.; Liu, S. *J. Med. Chem.* **2008**, *51*, 2971–2984.
(7) Yang, C. T.; Kim, Y. S.; Wang, J.; Wang, L.; Shi, J.; Li, Z. B.; Chen, X.; Fan, M.; Li, J. J.; Liu, S. *Bioconjug. Chem.* **2008**, *19*, 2008–2022.
(8) Liu, S. *Chem. Soc. Rev.* **2004**, *33*, 445–461.
(9) Rajander, J.; Schlesinger, J.; Avila-Rodriguez, M. A.; Solin, O. *J. Labelled Compd. Radiopharm.* **2009**, *52*, S234.
(10) Krupcik, J.; Oswald, P.; Majek, P.; Sandra, P.; Armstrong, D. W. *J. Chromatogr., A* **2003**, *1000*, 779–800.
(11) Schlesinger, J.; Koezle, I.; Bergmann, R.; Tamburini, S.; Bolzati, C.; Tisato, F.; Noll, B.; Klussmann, S.; Vonhoff, S.; Wuest, F.; Pietzsch, H.-J.; Steinbach, J. *Bioconjug. Chem.* **2008**, *19*, 928–939.
(12) Kotek, J.; Lubal, P.; Hermann, P.; Cisarova, I.; Lukes, I.; Godula, T.; Svobodova, I.; Taborsky, P.; Havel, J. *Chem.—Eur. J.* **2003**, *9*, 233–248.
(13) Van der Merwe, M. J.; Boeyens, J. C. A.; Hancock, R. D. *Inorg. Chem.* **1985**, *24*, 1208–1213.
(14) Wieghardt, K.; Bossek, U.; Chaudhuri, P.; Herrmann, W.; Menke, B. C.; Weiss, J. *Inorg. Chem.* **1982**, *21*, 4308–4314.
(15) Bevilacqua, A.; Gelb, R. I.; Hebard, W. B.; Zompa, L. J. *Inorg. Chem.* **1987**, *26*, 2699–2706.
(16) Geraldes, C. F. G. C.; Marques, M. P. M.; de Castro, B.; Pereira, E. *Eur. J. Inorg. Chem.* **2000**, 559–565.
(17) Meyer, M.; Dahaoui-Gindrey, V.; Lecomte, C.; Guilard, L. *Coord. Chem. Rev.* **1998**, *180*, 1313–1405.
(18) Di Bari, L.; Salvadori, P. *Coord. Chem. Rev.* **2005**, *249*, 2854–2879.
(19) Woods, M.; Kovacs, Z.; Kiraly, R.; Brucher, E.; Zhang, S.; Sherry, A. D. *Inorg. Chem.* **2004**, *43*, 2845–2851.